1 **Modeling of hepatitis B virus infection spread in primary human hepatocytes**

2
3 Zhenzhen Shi[1], Masataka Tsuge[1,2,3#], Nicholson Collier[4,5], Yasue Takeuchi[6], Takuro
4 Uchida[7], Carolyn M. Rutter[8], Yuji Teraoka[9], Susan Uprichard[1], Yuji Ishida[10], Chise
5 Tateno[10], Jonathan Ozik[4,5], Harel Dahari[1#], Kazuaki Chayama[11,12]
6
7 [1]The Program for Experimental & Theoretical Modeling, Division of Hepatology,
8 Department of Medicine, Loyola University Medical Center, Maywood, IL, USA. [2]Liver
9 Center, Hiroshima University Hospital, Hiroshima, Japan. [3]Department of
10 Gastroenterology, Graduate School of Biomedical & Health Sciences, Hiroshima
11 University, Hiroshima, Japan. [4]Consortium for Advanced Science and Engineering,
12 University of Chicago, Chicago, IL, USA. [5]Decision and Infrastructure Sciences,
13 Argonne National Laboratory, Argonne, IL, USA. [6]Hepatitis Information Center, The
14 Research Center for Hepatitis and Immunology, National Center for Global Health and
15 Medicine, Ichikawa, Chiba, Japan. [7]Division of Travel Medicine and Health, Research
16 Center for GLOBAL and LOCAL Infectious Diseases, Oita University, Yufu, Japan. [8],
17 Fred Hutchinson Cancer Research Center, Hutchinson Institute for Cancer Outcomes
18 Research, Biostatistics Program, Public Health Sciences Division, Seattle, WA,
19 USA.[9]Gastroenterology, National Hospital Organization Kure Medical Center and
20 Chugoku Cancer Center, Kure, Japan. [10]PhoenixBio Co., Ltd., Higashi-Hiroshima,
21 Japan. [11]Hiroshima Institute of Life Sciences, Hiroshima, Japan. [12]RIKEN Center for
22 Integrative Medical Sciences, Yokohama, Japan.
23
24 **#Corresponding authors:**
25 Masataka Tsuge, MD, PhD
26 Liver Center, Hiroshima University Hospital, 1-2-3 Kasumi, Minami-ku, Hiroshima, 734-
27 8551, Japan.
28 Tel: +81-82-257-2023. Fax: +81-82-257-2023
29 E-mail: tsuge@hiroshima-u.ac.jp
30
31
32 Harel Dahari, PhD
33 The Program for Experimental & Theoretical Modeling, Division of Hepatology,
34 Department of Medicine, Loyola University Medical Center, Maywood, IL, USA.
35 Tel: +1-708-216-4682. Fax: +1-708-216-6299
36 E-mail: hdahari@luc.edu

37

38 **word count** (abstract): 246 words; **word count** (main text) 4915 words:

39

Abstract

Chronic hepatitis B virus (HBV) infection poses a significant global health threat, causing severe liver diseases including cirrhosis and hepatocellular carcinoma. We characterized HBV DNA kinetics in primary human hepatocytes (PHH) over 32 days post-inoculation (pi) and used agent-based modeling (ABM) to gain insights into HBV lifecycle and spread. Parallel PHH cultures were mock-treated or HBV entry inhibitor Myr-preS1 (6.25 µg/mL) was initiated 24h pi. In untreated PHH, 3 viral DNA kinetic patterns were identified: (1) an initial decline, followed by (2) rapid amplification, and (3) slower amplification/accumulation. In the presence of Myr-preS1, viral DNA and infected cell numbers in phase 3 were effectively blocked, with minimal to no increase. This suggests that phase 2 represents viral amplification in initially infected cells, while phase 3 corresponds to viral spread to naïve cells. The ABM reproduced well the HBV kinetic patterns observed and predicted that the viral eclipse phase lasts between 18 and 38 hours. After the eclipse phase, the viral production rate increases over time, starting with a slow production cycle of 1 virion per day, which gradually accelerates to 1 virion per hour after 3 days. Approximately 4 days later, virion production reaches a steady state production rate of 4 virions/hour. The estimated median efficacy of Myr-preS1 in blocking HBV spread was 91% (range: 90-92%). The HBV kinetics and the predicted estimates of the HBV eclipse phase duration and HBV production cycles in PHH are similar of those predicted in uPA/SCID mice with human livers.

60

61 ***Importance*** While primary human hepatocytes (PHH) are the most physiologically

62 relevant culture system for studying HBV infection *in vitro*, comprehensive

63 understanding of HBV infection kinetics and spread in PHH is lacking. In this study, we

64 characterize HBV viral kinetics and employ agent-based modeling (ABM) to provide

65 quantitative insights into the HBV production cycle and viral spread in PHH. The ABM

66 provides an estimate of HBV eclipse phase duration, HBV production cycles and Myr-

67 preS1 efficacy in blocking HBV spread in PHH. The results resemble those predicted in

68 uPA/SCID mice with human livers, demonstrating that estimated HBV infection kinetic

69 parameters in PHH *in vitro* mirrors that observed in *in vivo* HBV infection chimeric

70 mouse model.

71

74

Introduction

76 An estimated 254 million people are chronically infected with hepatitis B virus (HBV),

77 with 1.2 million new infections reported annually (1). HBV infection leads to

78 approximately 1.1 million deaths each year, primarily due to HBV-related liver disease

79 such as cirrhosis and hepatocellular carcinoma (1). Current treatment options for

80 chronic hepatitis B include antiviral therapy with nucleoside/nucleotide analogues

81 (NUCs) and/or pegylated interferon alpha (2, 3). Although these treatments can

82 suppress HBV replication and slow the progression of liver disease, they do not cure the

83 infection. To develop more effective antiviral therapies aimed at eradicating HBV, it is

84 essential to better understand HBV lifecycle and spread (4).

85 Primary human hepatocytes (PHH) are well known for their high susceptibility to

86 HBV infection and their utility in molecular studies of HBV lifecycle (5). However, only a

87 few studies have utilized PHH cultures to examine HBV viral kinetics, and

88 comprehensive data on viral dynamics and the kinetics of HBV spread remain scarce

89 (6-8).

90 Mathematical modeling of HBV infection and treatment plays an important role in

91 elucidating the interactions between HBV and its host (9-13). Recent modeling of HBV

92 propagation from infection to steady state in humanized mice has emphasized the

93 significance of viral production cycles within individual cells for understanding the

94 complex, multiphasic kinetics of HBV infection *in vivo* (14). However, to date, there has

95 been no modeling of HBV spread in PHH.

96   In this study, we aimed to characterize the kinetics of HBV infection by

97   monitoring DNA at frequent time points and tracking HBV spread by monitoring the

98   number of infected cells over 32 days post inoculation (p.i.) in PHH in the absence or

99   presence of the HBV entry inhibitor Myr-preS1. Modeling was performed by adapting

100   the recently developed ABM of HBV infection in humanized mice to simulate HBV-host

101   interactions in PHHs (14), incorporating media replenishment and calibrating the model

102   with measured HBV DNA and HBV-infected cell spread. We identified three distinct

103   phases of both extracellular and intracellular HBV DNA kinetics. The ABM predicted that

104   Myr-preS1 treatment is highly effective (91%) in blocking viral spread, as evidenced by

105   an extremely slow increase in the third phase of both extracellular and intracellular HBV

106   DNA kinetics. The model estimates also demonstrated that HBV infection dynamics in

107   PHH in vitro closely mirrors that observed in the in vivo humanized liver chimeric mouse

108   model.

109

Results

HBV infection of PHH *in vitro* reveals three extracellular HBV DNA kinetic phases.

112   To characterize HBV kinetics in PHH up to 32 days p.i., 4 independent experiments

113   were performed (see Materials and Methods). Extracellular HBV DNA was measured

114   via qPCR revealing 3 kinetic phases consisting of a rapid decline (phase 1), a rapid

115   increase (phase 2), and slow increase (phase 3) (**Fig. 1**, blue lines; **Table 1**). In Exp.1,

116   there was a rapid decline phase with a slope of -0.82 $\log_{10}$/day ($t_{1/2}$=8.8hr, 95% CI, [7.7,

117   10.2]) until day 3 p.i., followed by a rapid increase phase with a slope of ~0.46 $\log_{10}$/day

118   (t_2=15.6hr, 95% CI, [14.7, 16.7]) between days 3-7 p.i., followed by a slower increase

119   phase with a slope of ~0.12 $\log_{10}$/day (t_2=59.9hr, 95% CI, [53.3, 68.3]) between days 7-

120   12 p.i. (**Fig. 1A**). Similar to Exp.1, the extracellular HBV DNA in Exp.2 increased rapidly

121   with a slope of ~0.51 $\log_{10}$/day (t_2=14.2hr, 95% CI, [13.4, 15.0]) from day 3-7 p.i.,

122   followed by a slower increase with a slope of ~0.15 $\log_{10}$/day (t_2=49.6hr, 95% CI, [41.8,

123   61.0]) from days 7-12 p.i. (**Fig. 1B**). In Exp.3, a slow increase was seen from days 12-

124   32 p.i. with a slope of ~0.09 $\log_{10}$/day (t_2=82.5hr, 95% CI, [78.6, 86.7]) (**Fig. 1C**). In

125   Exp.4, which was initiated at lower MOI to provide a detailed longitudinal kinetic picture,

126   the initial decline had a slope of -0.18 $\log_{10}$/day ($t_{1/2}$=40.1hr, 95% CI, [35.0, 46.9]) until

127   day 5 p.i.. This was followed by an increase with a slope of ~0.17 $\log_{10}$/day (t_2=42.8hr,

128   95% CI, [40.54, 45.29]) between days 5-17 p.i.. Thereafter, extracellular HBV DNA had

129   a slower increase with a slope of ~0.07 $\log_{10}$/day (t_2=102.7hr, 95% CI, [93.3, 114.3])

130   from days 17-32 p.i. (**Fig. 1D**). Thus, as observed in our previous *in vivo* HBV infection

131   in chimeric mice, the kinetics of extracellular HBV DNA was delayed in Exp.4 (GE=1)

132   compared to the Exps.1-3 where the inoculum was a log higher (GE=10).

133

134   **Intracellular HBV DNA kinetics during infection of PHH *in vitro* mirrors the same**

135   **three phases as extracellular HBV DNA.**

136   To characterize HBV intracellular kinetics in PHH up to 32 days post inoculation (p.i.),

137   cell lysates were collected at each time point in the 4 experiments and total HBV DNA

138   was measured via qPCR. Analogous to what was observed for extracellular HBV DNA,

139   three phases of cell-associated HBV DNA kinetics were identified: rapid decline (phase

140   1), rapid increase (phase 2), and slow increase (phase 3) (**Fig. 2**, black lines and **Table**

141   **2**). In Exp.1, cell-associated HBV DNA declined with a slope of -0.23 $\log_{10}$/day

6

142   ($t_{1/2}$=31.7hr, 95% CI, [28.4, 35.8]) from days 1-3 p.i.. Thereafter, intracellular HBV DNA

143   increased rapidly with a slope of ~0.38 $\log_{10}$/day (t_2=19.1hr, 95% CI, [17.2, 21.5]) from

144   days 3-7 p.i., followed by a slower increase phase with a slope of ~0.10 $\log_{10}$/day

145   (t_2=74.3hr, 95% CI, [63.6, 89.4]) from day 7 onwards (**Fig. 2A**). Likewise, in Exp.2, the

146   intracellular HBV DNA rapidly increased with a slope of ~0.42 $\log_{10}$/day (t_2=17.2hr, 95%

147   CI, [16.9, 17.4]) from days 3-7 p.i., followed by a slower increase with a slope of ~0.12

148     $\log_{10}$/day (t_2=59.4hr, 95% CI, [54.0, 66.0]) until day 12 p.i.. (**Fig. 2B**). Similar to the

149   slower amplification phase of Exps. 1 and 2, the intracellular HBV DNA increased slowly

150   with a slope of ~0.08 $\log_{10}$/day (t_2=92.1hr, 95% CI, [86.8, 98.2]) from days 12-2 p.i. in

151   Exp.3 (**Fig. 2C**). Although initiated at a lower MOI of 1, we observed a similar kinetics of

152   cellular HBV DNA in Exp.4: first phase decline slope of -0.18 $\log_{10}$/day ($t_{1/2}$=39.4hr, 95%

153   CI, [33.0, 49.1]) until day 3 p.i., followed by a fast increase with a slope of ~0.19

154     $\log_{10}$/day (t_2=39.0hr, 95% CI, [35.8, 42.8]) between days 3-7 p.i., followed by a slower

155   increase with a slope of ~ 0.08 $\log_{10}$/day (t_2=87.3hr, 95% CI, [82.2, 93.0]) from days 7-

156   32 p.i. (**Fig. 2D**).

157

158   **Myr-preS1 treatment affects the third phase of both intracellular and extracellular**

159   **HBV DNA kinetics.**

160   To determine the effect of blocking NTCP-mediated HBV entry in the 4 experiments

161   performed, parallel cultures were treated with Myr-preS1 to block NTCP-mediated HBV

162   entry starting 24h after HBV inoculation. Under Myr-preS1 treatment, extracellular HBV

163   DNA kinetics in Exp.1 followed the same three phases: (phase 1) rapid decline with a

164   slope of -0.93 $\log_{10}$/day ($t_{1/2}$=7.8hr, 95% CI, [7.2, 8.4]) until day 3 p.i.; (phase 2) fast

165　　increase with a slope of ~ 0.46 $\log_{10}$/day (t_2=15.7hr, 95% CI, [14.4, 17.3]) between days

166　　3-7 p.i.; and (phase 3) a slower increase with a slope of ~0.09 $\log_{10}$/day (t_2=84.8hr, 95%

167　　CI, [67.0, 115.6]) from day 7 onwards (**Fig. 1A**, red line). However, the last phase viral

168　　increase appeared slower and/or plateaued under Myr-preS1 treatment (**Fig. 1A**, red

169　　line), reduced from the ~0.12 $\log_{10}$/day (t_2=59.9hr, 95% CI, [53.3, 68.3]) increase

170　　observed in the absence of Myr-S1 (**Fig. 1A**, blue line). The same pattern was observed

171　　in Exp.2, with the slope between days 7-12 p.i. reduced from ~0.15 $\log_{10}$/day (t_2=49.6hr,

172　　95% CI, [41.8, 61.0]) to 0.10 $\log_{10}$/day (t_2=69.7hr, 95% CI, [59.8, 83.5]) in the presence

173　　of Mry-preS1 (**Fig. 1B**, blue vs. red line). Looking at days 12-32 p.i. in Exp.3, there was

174　　a much slower increase in extracellular HBV DNA in the presence Mry-preS1

175　　(slope=0.01 $\log_{10}$/day; t_2=583.6hr, 95% CI, [490.9, 719.5]) compared to untreated

176　　cultures (slope=0.09 $\log_{10}$/day; t_2=82.5hr, 95% CI, [78.6, 86.7]) (**Fig. 1C**). Likewise, in

177　　Exp.4, the third phase amplification was remarkably slower in the presence of Myr-

178　　pres1 (slope=0.02 $\log_{10}$/day; t_2=426.4hr, 95% CI, [324.7, 621.1]) compared to that

179　　observed in the untreated cultures (slope = 0.07 $\log_{10}$/day; t_2=102.7hr, 95% CI, [93.3,

180　　114.3]) (**Fig. 1D**).

181　　　　To determine how blocking NTCP-mediated HBV entry in the 4 experiments

182　　impact intracellular HBV DNA kinetics, cell lysates were harvested from the Myr-preS1

183　　treated cultures in all 4 experiments and cell-associated HBV DNA was measured via

184　　qPCR. Under Myr-preS1 treatment, intracellular HBV kinetics in Exp.1 follow three

185　　phases: (1) rapidly decline with a slope of -0.34 $\log_{10}$/day ($t_{1/2}$=20.95hr, 95% CI, [18.54,

186　　24.08]) until day 3 p.i.; (2) fast increase with a slope of ~ 0.37 $\log_{10}$/day (t_2=19.5hr, 95%

187　　CI, [17.6, 22.0]) between days 3-7 p.i.; (3) slow increase with a slope of ~0.05 $\log_{10}$/day

188   (t_2=147.8hr, 95% CI, [119.2, 194.6]) from day 7 onwards. While Phase 1 and 2 were

189   equivalent to the untreated cultures, Phase 3 had a considerably lower slope under Myr-

190   preS1 treatments. The same pattern was observed in the other experiments. In Exp.2,

191   intracellular HBV kinetics had a slower increase under Mry-preS1 treatment with a slope

192   of 0.08 $\log_{10}$/day (t_2=91.0hr, 95% CI, [79.4, 106.6]) between days 7-12 p.i.. In Exp.3, an

193   extremely slow increase during phase 3 was observed under Myr-preS1 compared to

194   untreated PHH (slope=~0.01 $\log_{10}$/day; t_2=501.20hr, 95% CI, [282.56, 2215.51] vs.

195   ~0.08 $\log_{10}$/day t_2=92.10hr, 95% CI, [86.76, 98.14]) (**Fig. 1C**). In Exp.4, the Phase 3

196   slope under Mry-preS1 was 0.01 $\log_{10}$/day; t_2=551.9hr, 95% CI, [407.8, 853.8]

197   compared to the untreated culture Phase 3 slope ~ 0.08 $\log_{10}$/day (t_2=87.3hr, 95% CI,

198   [82.2, 93.0]) (**Fig. 2D** and **Table 2**).

199

200   **Effect of Myr-preS1 reveals that the third phase of extracellular HBV infection in**

201   **PHH *in vitro* represents viral spread.**

202   Because Myr-preS1 is expected to block HBV spread to new PHH, we fixed parallel

203   cultures at the indicated time points in Exp.3 and Exp.4 to quantify the percentage of

204   HBV-infected cells in untreated and Myr-preS1 treated cultures (**Fig. 1,** blue versus red

205   boxplots, respectively). In Exp.3 on day 12 p.i., the mean percentage of HBV-infected

206   cells in Myr-preS1-treated and untreated cultures was equivalent (29.9% ± 4.1% vs.

207   27.7% ± 3.9, respectively) (**Fig. 1C**). However, the percentage of HBV-positive cells

208   was statistically lower under Myr-preS1 treatment compared to the untreated group on

209   day 32 p.i. (36.2% ± 4.1% vs. 95.6% ± 0.4%, respectively) (**Fig. 1C**). Similarly, in Exp.4

210   there was no difference in the percentage HBV-infected cells between Mry-preS1-

9

211   treated and untreated cells on day 12 p.i. (1.8% ± 1.9% vs. 2.0% ± 1.0%, respectively),

212   but was a significant difference in the percentage of HBV-infected cells on day 32 p.i.

213   (4.3% ± 1.4% vs. 80.7% ± 4.6%) (**Fig. 1D**). Together this demonstrates that Phase 3

214   primarily represents NTCP-dependent HBV spread.

215

216   **Model reproduces the kinetics of HBV infection observed in PHH and suggests**

217   **high Myr-preS1 efficacy in blocking HBV spread.**

218   To capture the kinetics of HBV *in vitro* in PHH, we adapted our recently developed ABM

219   and calibrated it with extracellular HBV data measured in Exp.4. Because Exp.4 has the

220   most complete HBV infection kinetics within a single experiment, we assessed whether

221   the model could fit the HBV kinetics observed in Exp.4, and the model reproduced well

222   the extracellular HBV DNA multiphasic pattern (**Fig. 3A** and **3B**) observed as well as the

223   percent infected cell data (**Fig. 3C** and **3D**). In addition, the oscillatory pattern of

224   extracellular HBV DNA kinetics predicted in the ABM reflected well the media changes

225   when the extracellular HBV DNA dramatically declined (**Fig. 3A** and **3B**). The ABM was

226   calibrated, resulting in sampled joint posteriors (**Fig. S1**, upper and lower rectangles)

227   and marginal parameter distributions (**Fig. S1**, diagonal rectangles) of all the model

228   parameters, both non-intervention and Myr-preS1 intervention parameters. We used a

229   calibration stopping criterion of 1000 effective sample size within the final calibration

230   target bounds. These results reveal the parameter ranges for HBV infection and

231   production and their high probability regions within those ranges that correspond to

232   simulated target values consistent with the empirical targets. They also depict

233   correlations between the infection-associated parameters (e.g., between ρ and β).

234   These modeling results estimate that the viral intracellular eclipse phase lasts

235   between 18-38 hours (**Table 3**). This non-productive eclipse phase ends and the P

236   phase begins when the model predicts an increase in the intracellular viral production

237   characterized by faster production cycles that release larger amounts of virus (**Fig. 4**).

238   Specifically, during the first 2.5 days p.i., the model predicted that infected PHH have a

239   long production cycle of 1 virion per day, but by 4 days p.i., infected PHH produce

240   virions faster with a rate of 2 virion per hour. During the eclipse stage, virion

241   production/release is minimal, so extracellular HBV DNA levels are observed to

242   decrease consistent with the media removal/replenishment occurring at days 1 and 3

243   p.i.. After day 4 p.i., the virion production in each cell reaches a steady-state production

244   rate of 4 virions per hour leading to an increase in virion release and infection of new

245   PHH that explains the fast extracellular HBV DNA increase observed between days 5-

246   17 p.i.. Then, as the number of target PHH decreases the extracellular HBV DNA

247   increase slows consistent with the third phase of slower amplification. Again, looking at

248   Exp.4, the model recapitulated the much slower increase in extracellular HBV DNA from

249   days 12-32 p.i. under Myr-preS1 treatment (**Fig. 3B** and **3D**). Based on the calibration,

250   the ABM predicts a median Myr-preS1 efficacy of 91.0% (first quantile [Q1]: 90% - third

251   quantile [Q3]: 92%) to be achieved after a median 54 hours (Q1:40 hr – Q3:65 hr) post

252   treatment initiation, suggesting a high efficacy of Myr-preS1 treatment in blocking HBV

253   spread at an early stage of infection.

254

Discussion

In this study, we characterized the viral kinetics of HBV infection and assessed viral spread over a period of 32 days in PHH. We identified three distinct phases in both extracellular and intracellular HBV DNA kinetics: a first rapid decline, a second rapid increase, and a third slow increase phase. Notably, the second rapid and third slow increase phases observed in PHH closely resemble the two amplification phases (phase 4 and 6) seen in the humanized mouse model (14). We show that the ABM reproduces well the measured viral DNA kinetic and spread data by assuming a cyclic nature of viral production, characterized by an initial slow but increasing rate of HBV production in individual cells, consistent with the modeling findings during acute HBV infection in humanized mice (14). The ABM also predicts that Myr-preS1 treatment is highly effective (91±1%) in blocking viral spread, as evidenced by an extremely slow increase in the third phase of both extracellular and intracellular HBV DNA kinetics.

Although extracellular and intracellular HBV DNA exhibited similar kinetic patterns across 4 experiments, a more detailed analysis of viral kinetics under varying HBV inocula dose revealed notable differences. First, the extracellular HBV DNA level in Exp.1 declined approximately five times faster (−0.82 log10/day) than in Exp.4 (−0.18 log10/day) (**Table 1**). Given that that HBV degradation is relatively stable in media (15), the faster decline in Exp.1 might suggest an unexpectedly higher rate of HBV removal from the media by media replenishment. In addition, the rapid increase phase in Exp.1 occurred ~3 times faster (0.46 $\log_{10}$/day) compared to Exp.4 (0.17 $\log_{10}$/day) (**Table 1**), Because higher inoculum HBV levels (GE=10 in Exp.1 > GE=1 in Exp.4) is expected to result in higher viral uptake, this suggests that a higher initial HBV levels (perhaps within

12

278   individual cells) may lead to more efficient virion production and/or faster viral spread,

279   as evidenced by a two-fold faster rapid increase phase of intracellular HBV DNA in

280   Exp.1 (0.38 $\log_{10}$/day) compared to Exp.4 (0.19 $\log_{10}$/day) (**Table 2**).

281   To the best of our knowledge, HBV spread in PHH has not been investigated in

282   previous studies. The lack of increase in extracellular HBV DNA, intracellular HBV DNA,

283   and the number of infected cells during phase 3 in the presence of Myr-preS1 suggests

284   that phase 2 reflects viral amplification within initially infected cells, while phase 3

285   represents the spread to naïve cells. Consequently, phase 3 of intracellular HBV

286   amplification, in the absence of Myr-preS1, parallels the spread observed in

287   extracellular HBV kinetics. The continued, though slower, increase in intracellular HBV

288   levels (with a slope of 0.01-0.08 log10/day; Table 2) during phase 3 in the presence of

289   Myr-preS1 suggests either incomplete inhibition of viral spread or that intracellular HBV

290   levels had not yet reached steady state.

291   To better understand the HBV kinetics observed in PHH, we adapted our recently

292   developed ABM by incorporating media replenishment and accounting for the impact of

293   Myr-preS1 interventions on HBV spread. We estimated several key parameters that

294   reflect both the duration of the HBV eclipse phase and its subsequent production cycles.

295   Interestingly, our results showed that the duration of the HBV eclipse phase in PHH

296   ranges from 18 to 38 hours, a more narrow and consistent range compared to the 7-50

297   hour duration predicted for the chimeric mouse model (14). The model's estimate for

298   virion production at steady state (i.e., P_{st}) is identical in both systems, with

299   approximately 4 virions per infected cell per hour in PHH and in mice. Other key

300   parameters related to the viral production cycle, such as initial production cycle length

13

301   (20-27hr in PHH vs. 23-30hr in humanized mice), the number of viral production cycles

302   to reach 50% of P_{st} (15-26 in PHH vs. 14-30 in humanized mice), and the steepness of

303   the production curves (0.50-0.60hr^{-1} in PHH vs. 0.40-0.60hr^{-1} in humanized mice), also

304   show similarities, further suggesting that HBV infection kinetics in PHH closely resemble

305   those in the chimeric mouse model. This similarity indicates that viral replication is

306   similarly regulated in human hepatocytes *in vitro* and *in vivo*. While it is acknowledged

307   that *in vitro* experiments lack the physiological benefits of *in vivo* systems—such as the

308   influence of proteins from other organs, including cytokines, chemokines, and

309   hormones—these *in vitro* models offer a valuable platform for analyzing the detailed

310   dynamics of HBV replication, free from the confounding effects of such factors.

311   HBV infects hepatocytes by first attaching to heparan sulfate proteoglycans

312   (HSPGs) and subsequently binding to the HBV receptor, human sodium taurocholate

313   co-transporting polypeptide (hNTCP). We employed treatment with Myr-preS1 entry

314   inhibitor, to block viral binding to hNTCP by competitive inhibition. To assess its efficacy

315   in PHH, Myr-preS1 was administered starting one day post-inoculation to prevent the

316   spread of HBV infection. The model predicts that the fraction of HBV-infected cells

317   increased very slowly, from approximately 2-7%, between days 17-32 p.i., suggesting

318   that Myr-preS1 effectively interfered with HBV spread (**Fig. 3D**). The estimated median

319   efficacy of Myr-preS1 treatment was 91%, indicating that (1) higher dosages may be

320   required to fully block HBV infection, (2) HBV may interact with other receptors during

321   cell entry, and/or (3) additional spread mechanisms (e.g., spread to adjacent cells,

322   forming infected cell clusters (16)), may contribute to further HBV infection at later

323   stages. The lack of decline in intracellular HBV DNA under Myr-preS1 treatment

14

324   suggests that HBV infection remains stable in the absence of re-infection, which also

325   implies that cccDNA maintenance is not dependent on re-infection under these

326   conditions. However, with the cccDNA half-life predicted to be approximately 40 days in

327   vitro, longer-term experiments are needed to confirm these findings.

328   Our study has several limitations. First, we used only Exp.4 for modeling, as

329   Experiments 1 to 3 had less frequent data sampling, which limited our ability to model

330   the differences in HBV kinetics at varying HBV input doses. Future experimental work

331   with more frequent sampling points is needed to compare HBV viral kinetics across

332   different doses. Second, we did not include intracellular HBV DNA or cccDNA in the

333   model for the sake of simplicity. To gain a deeper understanding of intracellular HBV

334   dynamics, an integration of the current ABM with our recent mathematical model that

335   accounts for intracellular viral DNA and cccDNA kinetics (15) is warranted. Lastly, PHH

336   death was not incorporated into the ABM. In our PHH culture system, although cell

337   density slightly decreased by day 2 p.i., the number of hepatocytes remained stable for

338   at least 33 days (17). Based on these observations and for model simplification, we

339   assumed that excluding PHH loss or death would not significantly affect the results.

340   However, for longer-term experiments monitoring HBV infection in PHH, the inclusion of

341   cell death and PHH loss may be necessary for accurately calibrating HBV kinetics in the

342   model.

343   In conclusion, this study demonstrates that HBV DNA levels follow multiphasic

344   replication kinetics in PHH. Myr-preS1 treatment effectively blocks HBV spread,

345   although it does not prevent it completely. By comparing model predictions from both

346   the in vivo humanized mouse model and the in vitro PHH system, we show that HBV

347   infection dynamics in PHH closely mirror those observed in the uPA/SCID chimeric

348   mouse model, suggesting that there are virtually no other factors in this mouse model

349   that impacting HBV spread. Future studies, including mathematical modeling of

350   intracellular replication and cccDNA transcription, will provide deeper insights into HBV

351   spread and HBV-host dynamics at the molecular level.

352

353   **Materials and Methods**

354   **PHH Preparation**

355   Commercially available cryopreserved human hepatocytes (BD Bioscience, lot195,

356   Hispanic, female, 2 years) were transplanted into cDNA-uPA/SCID mice via injection

357   into the spleen. PHH were isolated from the chimeric mice with humanized livers at 9-15

358   weeks after transplantation by a standard collagenase perfusion. To expand the cells,

359   the isolated PHH were serially transplanted into additional cDNA-uPA/SCID mice as

360   previously described (18). Nine to fifteen weeks after the serial transplantation, PHH

361   were collected for in vitro culture and infection. PHH were seed in collagen-coated 24

362   well plates (Corning, Japan) at 2.0×10^5 cells/well (Exp.1) and 4.0×10^5 cells/well (Exp.2

363   and 4) or in 48 well plates at 1.6×10^5 cells/well (Exp.3) and incubated at $37C^o$ with 5%

364   CO_2 in dHCGM medium (**Table 4**). The base of this medium is Dulbecco's modified

365   Eagle' medium (Gibco ThermoFisher Scientific) supplemented with 44mM NaHCO3

366   (Wako Chemicals), 100IU/ml Penicillin G (Invitrogen ThermoFisher Scientific),

367   100µg/mL Streptomycin (Invitrogen ThermoFisher Scientific), 20mM HEPES (Gibco

368   ThermoFisher Scientific), 10% FBS (Biosera), 15µg/mL L-proline (Wako Chemicals),

369   0.25µg/mL insulin (Sigma-Aldrich), 50nM Dexamethasone (Sigma-Aldrich), 5ng/mL

16

370 Epidermal growth factor (Sigma-Aldrich), 0.1mM L-ascorbic acid 2-phosphate (Wako

371 Chemicals), and 2% Dimethyl sulfoxide (Sigma-Aldrich).

372

HBV Inoculum

374 HBV genotype C2 obtained from a chronic hepatitis B patient and named Hiroshima

375 GtC CL3 (NCBI accession No. MH818373) was used as inoculum in this study. The

376 virus was amplified in cDNA-uPA/SCID mice as previously described (18).

377

HBV Infection

379 PHH were treated with an inoculum of 10 HBV GEq/cell (Exp.1-3) or 1 HBV GEq/cell

380 (Exp.4) for 1 day with 4% polyethylene glycol 8000 (PEG 8000). The inoculated cells

381 were cultured with 200 µL or 500 µL of culture medium for 48 well and 24 well plates,

382 respectively. Myr-preS1 (6.25 µg/mL) treatment was initiated one day after inoculation

383 and then continued throughout the experiment. Extracellular HBV DNA and intracelluar

384 HBV DNA were measured in replicate wells at the indicated time points for each

385 experiment. During the infection, culture media was renewed after HBV inoculation or

386 until the end of the experiment as indicated by arrows in **Fig. 5**.

387

Quantification of extracellular HBV DNA in culture medium

389 HBV DNA levels in culture media were quantified by qPCR as previously described (19).

390 DNA was extracted using SMI TEST (Genome Science Laboratories, Tokyo, Japan)

391 and dissolved in 20µL of H_2O. Real-time PCR analysis was performed using ABI Prism

392 7300 Sequence Detection System. Amplification was performed in a 25µL reaction

17

393   mixture containing SYBR Green PCR Master Mix (Applied Biosystems, Foster City, CA),

394   200nM of forward primer, 200nM of reverse primer, and 1µL of DNA or cDNA solution.

395   After incubation for 2 minutes at 50°C, the sample was heated for 10 minutes at 95°C

396   for denaturing, followed by a PCR cycling program consisting of 40 2-step cycles of 15

397   seconds at 95°C and 60 seconds at 60°C. The lower detection limit of this assay was

398   2.3 log copies/ml. The primers used for extraction are as follows: forward 5'-

399   TTTGGGGCATGGACATTGAC-3' and reverse 5'- GAGTGCTGTATGGTGAGGTG-3'.

400

401   **HBV DNA isolation and analysis**

402   DNA was extracted from the harvested PHH using SMITEST (Genome Science

403   Laboratories, Tokyo, Japan) in accordance with the manufacturer's instructions.

404   Intracellular HBV DNA and cccDNA levels were quantified by qPCR and TaqMan PCR,

405   respectively, using an ABI Prism 7300 (Applied Biosystems, Carlsbad, CA, USA), as

406   previously described (20). Briefly, the concentration of purified DNA was measured by

407   BioPhotometer® 6131 (Eppendorf, Tokyo, Japan). Intracellular HBV DNA was

408   quantified by qPCR using the same protocol and primers for extracellular HBV DNA

409   quantification. Single-stranded DNA was selectively degraded from the extracted DNA

410   using S1 nuclease (TakaraBio, Shiga, Japan), and then cccDNA levels were quantified.

411   For total HBV DNA the forward primer (nucleotides [nt] 1521-1545: 5-

412   GGGGCGCACCTCTCTTTACGCGGTC-3), reverse primer (nt 1862-1886: 5-

413   CAAGGCACAGCTTGGAGGCTTGAAC-3), and TaqMan MGB probe (nt 1685-1704: 5-

414   FAM-AACGACCGACCTTGAGGCAT-MGB-3) were utilized. PCR was performed using

415   100ng of extracted DNA, TaqMan® Fast Advanced Master Mix (Applied Biosystems),

416   300nmol of each primer and 250nmol of the probe. Amplification was performed as

417   follows: 50°C for 2 min, then 95°C for 10 min, followed by 45 cycles of 95°C for 10 sec,

418   58°C for 5 sec, 63°C for 10 sec, and 20 sec at 72°C. The lower limited detection was

419   100 copies/100ng DNA.

420

421   **Estimation of HBV infected cells**

422   Immunostaining for HBsAg was conducted as previously described (18). At indicated

423   times after inoculation, PHH were fixed with 10% formalin neutral buffer solution for 10

424   minutes at room temperature. After washing twice with PBS, the fixed PHHs were

425   treated with anti-HBsAg goat polyclonal antibody (bs-1557G ; Bioss Inc, Woburn, MA).

426   To analyze the percentage of HBsAg-positive PHH, five pictures were taken with a BZ-

427   X700 microscope (Keyence, Osaka, Japan) and the number of PHH and HBsAg-

428   positive PHH were counted.

429

430   **Modeling HBV dynamics**

431   To study HBV spread in PHH, we modified our recently developed ABM to describe

432   HBV infection in humanized mice (14). Analogous to the published model, this ABM

433   consists of two types of agents to account for the PHH and the extracellular virus. Here,

434   the PHH are represented by a two-dimensional grid of stationary cells while the virus is

435   represented by freely diffusing agents intended to represent the amount of HBV in the

436   culture medium. Each individual PHH can be in one of the following three discrete

437   states: uninfected/susceptible PHH targets (T), infected PHH in an eclipse phase (I_E), or

438   productively infected PHH secreting progeny virus (I_P) (**Fig. 6**). The ABM execution is

19

439   again an iterative process where each iteration represents a discrete time step, each

440   step = 1 hour. For each iteration, uninfected/susceptible PHH are infected and initially

441   enter an eclipse phase (I_E). After a random period of time following a uniform distribution

442   of $U(\Omega_{min}, \Omega_{max})$, the infected PHH proceeded from the eclipse phase to the productive

443   phase, and then they start to release newly generated progeny virus (i.e., I_p). The

444   magnitude and frequency of secreted virus is calculated using the following two

445   equations to mimic the cyclic nature of the viral lifecycle within each cell (**Eq.1** and **Eq.2**)

446
$$P(\tau) = \frac{P_{st}}{1+e^{-\gamma(\tau-\alpha)}} \qquad \text{(Eq.1)}$$

447   where $P(\tau)$ is number of virions produced by infected cells a τ, P_{st} is steady state virus

448   production, α is number of cycles to reach to 50% of P_{st}, γ is steepness of the

449   production curve, and τ is the production cycle

450
$$l_\tau = \delta e^{-\omega\tau} \qquad \text{(Eq.2)}$$

451   where l_τ is interval between production cycle, τ is the production cycle, δ is scaling

452   factor indicating the initial production cycle length, and ω is decay constant.

453   To account for the removal of virus containing media and replenishment with

454   fresh media, a removal/replenishment rate (*Rr*) was newly incorporated into the *in vitro*

455   ABM which estimates the percentage of extracellular virus removed at each media

456   change. To estimate the effect of the drug intervention on HBV spread, the following

457   step function (**Eq.3**) was also incorporated into the ABM

458
$$\eta(t) = \begin{cases} 0 & t < t_{eff} \\ \eta & t \geq t_{eff} \end{cases} \qquad \text{(Eq.3)}$$

459 where η is efficacy of Myr-preS1 and t_{eff} is time when Myr-preS1 starts to take effect. A

460 schematic picture of the modified agent-based model is shown in **Fig. 6**.

461

462 **Parameter estimation**

463 We previously showed that the degradation of extracellular HBV DNA *in vitro* is

464 extremely slow since the HBV is quite stable in the culture medium (21). Thus, in the

465 ABM we assumed a fixed virus clearance rate of 0.0004 h^{-1} ($t_{1/2}$ =72.2 days) in between

466 the media changes. To estimate the remaining parameters, we applied the following two

467 steps including preliminary AnyLogic fits and Incremental Mixture Approximate

468 Bayesian Computation (IMABC) (22). Removal/replenishment parameter *Rr* was

469 estimated to be in the range of (0.01-1) by fitting the ABM to the untreated PHH

470 experimental data using AnyLogic optimization tool. Parameter ranges for efficacy of

471 Myr-preS1 (η) and time when Myr-preS1 takes effect (t_{eff}) were estimated by fitting the

472 ABM to the experimental data under Myr-preS1 intervention. Parameter ranges for other

473 parameters were determined based on the *in vivo* mouse model (14). By assuming

474 uniform prior distributions for each parameter using the estimated ranges in the first

475 step, we applied IMABC to obtain the posterior distributions of parameters.

476

477 **Model calibration using IMABC**

478 The agent-based model (ABM) was calibrated by identifying parameters that result in

479 model predictions that fit the experimental data. We utilized the IMABC algorithm (22)

480 for calibration, implemented with the R IMABC package (23) and the EMEWS

481 framework (24) on Argonne's LCRC Bebop high-performance computing cluster. The

21

482   IMABC algorithm works by adaptively constraining model output target bounds. The

483   algorithm converges when a sufficient number of model parameters (effective sample

484   size, i.e., 1000 samples) are found to simulate targets within the final empirical target

485   bounds. During model calibration, two sets of ABM targets were sequentially evaluated,

486   corresponding to non-intervention and intervention data. The calibration algorithm first

487   used the ABM to simulate non-intervention targets (i.e., untreated PHH). If the non-

488   intervention ABM did not result in points within the non-intervention targets, the

489   parameter set was rejected. For each parameter vector that produced simulated targets

490   (**Table S1**) within the specified IMABC target bounds, the algorithm next evaluated fit to

491   intervention targets from the Myr-preS1 intervention. Through this approach the non-

492   intervention and intervention ABM parameters were simultaneously estimated.

505

506

507

Reference

1. Organization WH. 9 April 2024. Hepatitis B. https://www.who.int/news-room/fact-sheets/detail/hepatitis-b. Accessed

2. Ye J, Chen J. 2021. Interferon and hepatitis B: current and future perspectives. Frontiers in Immunology 12:733364.

3. Liaw Y-F, Papatheodoridis G. 2024. Finite nucleos (t) ide-analogue therapy for functional cure in HBeAg-negative chronic hepatitis B: recent development in the paradigm shift. Hepatology:10.1097.

4. Ploss A, Strick-Marchand H, Li W. 2021. Animal models for hepatitis B: does the supply meet the demand? Gastroenterology 160:1437-1442.

5. Hu J, Lin Y-Y, Chen P-J, Watashi K, Wakita T. 2019. Cell and animal models for studying hepatitis B virus infection and drug development. Gastroenterology 156:338-354.

6. Nosaka T, Naito T, Matsuda H, Ohtani M, Hiramatsu K, Nemoto T, Nishizawa T, Okamoto H, Nakamoto Y. 2020. Molecular signature of hepatitis B virus regulation by interferon-γ in primary human hepatocytes. Hepatology Research 50:292-302.

7. Lucifora J, Michelet M, Rivoire M, Protzer U, Durantel D, Zoulim F. 2020. Two-dimensional-cultures of primary human hepatocytes allow efficient HBV infection: Old tricks still work! Journal of hepatology 73:449-451.

8. Kitagawa K, Kim KS, Iwamoto M, Hayashi S, Park H, Nishiyama T, Nakamura N, Fujita Y, Nakaoka S, Aihara K. 2024. Multiscale modeling of HBV infection integrating intra-and intercellular viral propagation to analyze extracellular viral markers. PLOS Computational Biology 20:e1011238.

9. Reinharz V, Ishida Y, Tsuge M, Durso-Cain K, Chung TL, Tateno C, Perelson AS, Uprichard SL, Chayama K, Dahari H. 2021. Understanding hepatitis B virus dynamics and the antiviral effect of interferon alpha treatment in humanized chimeric mice. Journal of virology 95:10.1128/jvi. 00492-20.

536   10.   Kadelka S, Dahari H, Ciupe SM. 2021. Understanding the antiviral effects of
537   RNAi-based therapy in HBeAg-positive chronic hepatitis B infection. Scientific
538   Reports 11:200.
539   11.   Neumann AU, Phillips S, Levine I, Ijaz S, Dahari H, Eren R, Dagan S, Naoumov
540   NV. 2010. Novel mechanism of antibodies to hepatitis B virus in blocking viral
541   particle release from cells. Hepatology 52:875-885.
542   12.   Ciupe SM, Dahari H, Ploss A. 2024. Mathematical Models of Early Hepatitis B
543   Virus Dynamics in Humanized Mice. Bulletin of Mathematical Biology 86:53.
544   13.   Dahari H, Shudo E, Ribeiro RM, Perelson AS. 2009. Modeling complex decay
545   profiles of hepatitis B virus during antiviral therapy. Hepatology 49:32-38.
546   14.   Hailegiorgis A, Ishida Y, Collier N, Imamura M, Shi Z, Reinharz V, Tsuge M,
547   Barash D, Hiraga N, Yokomichi H. 2023. Modeling suggests that virion
548   production cycles within individual cells is key to understanding acute hepatitis B
549   virus infection kinetics. PLOS Computational Biology 19:e1011309.
550   15.   Shekhtman L, Ishida Y, Tsuge M, Reinharz V, Yamao M, Takahashi M, Tateno C,
551   Uprichard SL, Dahari H, Chayama K. 2024. Modelling of hepatitis B virus kinetics
552   and accumulation of cccDNA in primary human hepatocytes. JHEP
553   Reports:101311.
554   16.   König A, Yang J, Jo E, Park KHP, Kim H, Than TT, Song X, Qi X, Dai X, Park S.
555   2019. Efficient long-term amplification of hepatitis B virus isolates after infection
556   of slow proliferating HepG2-NTCP cells. Journal of hepatology 71:289-300.
557   17.   Yamasaki C, Ishida Y, Yanagi A, Yoshizane Y, Kojima Y, Ogawa Y, Kageyama Y,
558   Iwasaki Y, Ishida S, Chayama K. 2020. Culture density contributes to hepatic
559   functions of fresh human hepatocytes isolated from chimeric mice with
560   humanized livers: Novel, long-term, functional two-dimensional in vitro tool for
561   developing new drugs. PloS one 15:e0237809.
562   18.   Ishida Y, Yamasaki C, Yanagi A, Yoshizane Y, Fujikawa K, Watashi K, Abe H,
563   Wakita T, Hayes CN, Chayama K. 2015. Novel robust in vitro hepatitis B virus
564   infection model using fresh human hepatocytes isolated from humanized mice.
565   The American journal of pathology 185:1275-1285.

566   19.   Nomura M, Tsuge M, Uchida T, Hiraga N, Kurihara M, Tsushima K, Fujino H,
567   Nakahara T, Murakami E, Abe-Chayama H, Kawaoka T, Miki D, Hiramatsu A,
568   Imamura M, Kawakami Y, Aikata H, Ochi H, Zhang Y, Makokha GN, Hayes CN,
569   Tanaka S, Chayama K. 2018. CTL-associated and NK cell-associated immune
570   responses induce different HBV DNA reduction patterns in chronic hepatitis B
571   patients. J Viral Hepat 25:1555-1564.

572   20.   Tsuge M, Uchida T, Hiraga N, Kan H, Makokha GN, Abe-Chayama H, Miki D,
573   Imamura M, Ochi H, Hayes CN. 2017. Development of a novel site-specific
574   pegylated interferon beta for antiviral therapy of chronic hepatitis B virus.
575   Antimicrobial Agents and Chemotherapy 61:e00183-17.

576   21.   Than TT, Jo E, Todt D, Nguyen PH, Steinmann J, Steinmann E, Windisch MP.
577   2019. High environmental stability of hepatitis B virus and inactivation
578   requirements for chemical biocides. The Journal of infectious diseases 219:1044-
579   1048.

580   22.   Rutter CM, Ozik J, DeYoreo M, Collier N. 2019. Microsimulation model
581   calibration using incremental mixture approximate Bayesian computation. The
582   Annals of Applied Statistics 13:2189-2212.

583   23.   Maerzluft CE, Carolyn M. Rutter, Jonathan Ozik, and Nicholson Collier. . 2021.
584   Incremental Mixture Approximate Bayesian Computation (IMABC) [R Package
585   Imabc Version 1.0.0]. April 2021 https://CRANR-projectorg/package=imabc.

586   24.   Ozik J, Collier NT, Wozniak JM, Spagnuolo C. From desktop to large-scale
587   model exploration with Swift/T, p 206-220. In (ed), IEEE,

588

589

590 **Tables**

591   **TABLE 1** Detailed characterization of extracellular HBV kinetics under Exps. 1-4
592

Exp.#	Phase 1 Slope ($\log_{10}$/d) [95%CI]		Phase 2 Slope ($\log_{10}$/d) [95%CI]		Phase 3 Slope ($\log_{10}$/d) [95%CI]	
	Untreated	Myr-preS1	Untreated	Myr-preS1	Untreated	Myr-preS1
Exp.1	-0.82 [-0.94, -0.71]	-0.93 [-1.00, -0.86]	0.46 [0.43, 0.49]	0.46 [0.42,0.50]	0.12 [0.11, 0.14]	0.09 [0.06, 0.11]
Exp.2	NA	NA	0.51 [0.48, 0.54]	NA	0.15 [0.12, 0.17]	0.10 [0.09, 0.12]
Exp.3	NA	NA	NA	NA	0.09 [0.08, 0.09]	0.01 [0.01, 0.02]
Exp.4	-0.18 [-0.21, -0.15]	NA	0.17 [0.16, 0.18]	NA	0.07 [0.06, 0.08]	0.02 [0.01, 0.02]
NA, not available; CI, confidence interval.						

593

594   **TABLE 2** Detailed characterization of intracellular HBV kinetics under Exps. 1-4

595

Exp. #	Phase 1 Slope ($\log_{10}$/d) [95%CI]		Phase 2 Slope ($\log_{10}$/d) [95%CI]		Phase 3 Slope ($\log_{10}$/d) [95%CI]	
	Untreated	Myr-preS1	Untreated	Myr-preS1	Untreated	Myr-preS1
Exp.1	-0.23 [-0.25, -0.20]	-0.34 [-0.39, -30]	0.38 [0.34, 0.42]	0.37 [0.33, 0.41]	0.10 [0.08, 0.11]	0.05 [0.04, 0.06]
Exp.2	NA	NA	0.42 [0.41, 0.43]	NA	0.12 [0.11, 0.13]	0.08 [0.07, 0.09]
Exp.3	NA	NA	NA	NA	0.08 [0.07, 0.08]	0.01 [0.00, 0.03]
Exp.4	-0.18 [-0.22, -0.15]	NA	0.19 [0.17, 0.20]	NA	0.08 [0.08, 0.09]	0.01 [0.01, 0.02]
NA, not available; CI, confidence interval.						

596

TABLE 3 IMABC calibration for fitting Exp. 4 with and without Myr-preS1. Each parameter was sampled based on a uniform distribution (prior distribution) to implement IMABC. IQR represents the difference between the 25th and 75th percentiles of the marginal posterior distribution of parameters. All IMABC fits are shown in **Fig. 3**.

Category	Parameter description	Symbol [unit]	Prior simulations and preliminary fits (uniform)		IMABC calibration	
			[min-max]	Source	median	IQR [Q1-Q3]
Initial condition	Initial uninfected PHH number	T_0 [cell]	[38000-42000]	Expert opinion[1]	39900	[38874-41040]
	Initial viral load	V_0 [virion]	[15924-100475]	Expert opinion[1]	30662	[24779-37093]
Infection	Fraction of virion that are infectious	ρ	[0.145-0.58]	(14)	0.28	[0.19-0.33]
	Infection rate	β [cell/hr]	[0.0001-0.0025]	(14)	0.0009	[0.0005-0.0011]
Eclipse phase	Min eclipse phase	Ω_{min} [hr]	[5-36]	(14)	18	[12-26]
	Max eclipse phase	Ω_{max} [hr]	[18-50]	(14)	38	[30-45]
Production (Eq. 1 and Eq.2)	Initial production cycle length	δ [hr]	[15-30]	(14)	23.41	[19.62-27.19]
	Decay constant	ω [hr^{-1}]	[0.3-0.97]	(14)	0.54	[0.50-0.60]
	Number of cycles to reach 50% of P_{st}	α [hr]	[10-30]	(14)	21	[15-26]
	Steepness of the production curve	γ [hr^{-1}]	[0.1-0.9]	(14)	0.35	[0.26-0.48]
	Virus production at steady state	P_{st} [virion/cell/hr]	[2-5]	(14)	4	[3-4]
Media change	Removal rate	Rr	[0.01-1]	Educational fits[2]	0.75	[0.68-0.77]
Myr-preS1 treatment	Efficacy of Myr-preS1	η	[0.5-1]	Educational fits[2]	0.91	[0.90-0.92]
	Time at Myr-preS1 taking effect	t_{eff} [hr]	[24-72]	Educational fits[2]	54	[40-65]

Note:

1. Our experimentalists suggest that initial uninfected PHH number (T_0) in an individual well is from 3.8×10^5 to 4.2×10^5. To improve the computational efficiency, we used 1/10 of the actual number which is the range of 3.8×10^4 to 4.2×10^4 in the ABM to model the virus spread in the culture media. The initial viral load (V_0) is 4.0×10^5 per well which was rescaled to 4.0×10^4 to conform to the scaled-down PHH number. In addition, 0.4log was added to the lower and upper bounds of each viral measurement to account for experimental variations so the final range for the initial viral load is from 15924 (4.2log) to 100475 (5log).

2. The range was determined based on preliminary model fittings using AnyLogic optimization tool.

29

613

614 <div style="text-align:center">TABLE 4 Initial conditions for each experiment</div>

	Exp.1	Exp. 2	Exp.3	Exp.4
Number of Hepatocyte (cells/well)	2.0×10^5	4.0×10^5	1.6×10^5	4.0×10^5
Plate (well)	24	24	48	24
Volume of culture medium (uL/well)	500	500	200	500
MOI (genome equivalents/cell)	10	10	10	1

615
616
617

618

Figures

Fig. 1. Measured excellular HBV DNA and percentage of HBV-infected cells in Exps. 1 – 4 (A-D). Solid line represents the median value of excellular HBV DNA in the control group (blue) and under Myr-preS1 treatment (red). Errorbar denotes the minimal and maximiual measurments of excellular HBV DNA. Boxplot represents the percentage of HBV-infected cells (average±SD). Arrows indicate the media changes/replenishsment.

628
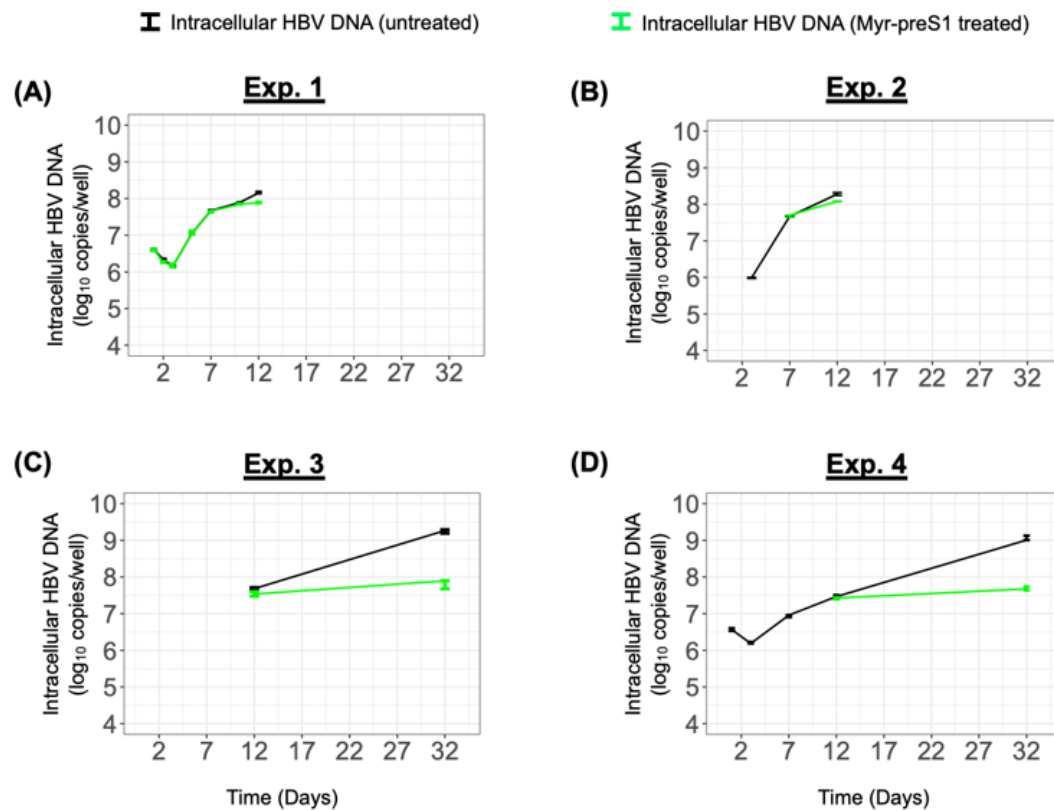
Fig. 2. Measured intracellular HBV DNA in Exps. 1 – 4 (A-D). Solid line represents the median value of intracellular HBV DNA in the control group (black) and under Myr-preS1 treatment (green). Errorbar denotes the minimal and maximual measurments of intracellular HBV DNA.
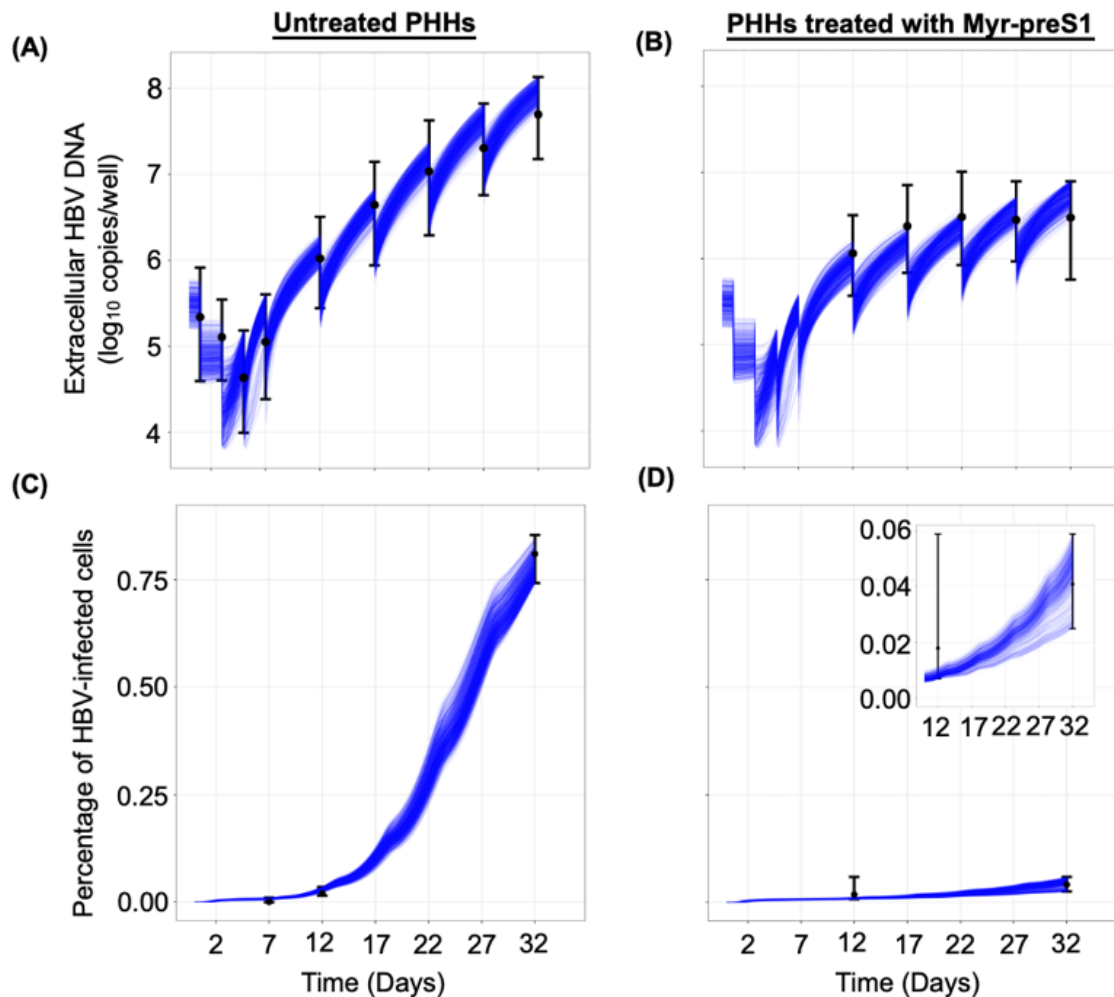
Fig. 3. ABM calibration by fitting to Exp. 4. (A-D). ABM simultaneous calibrations (blue solid curves) with measured extracellular HBV DNA (top) and percentage of HBV-infected PHH (bottom) in Exp. 4. Left panels (A & C): Untreated. Right panels (B & D): Myr-preS1 treated. The ABM calibrations were done using the IMABC algorithm. Black dots are the median empirical calibration target values (i.e., extracellular HBV DNA) for each time point, error bars are the minimal and maximal bounds for the empirical targets, and blue lines represent 1000 IMABC posterior outputs, all of which are contained with all of the empirical calibration bounds.
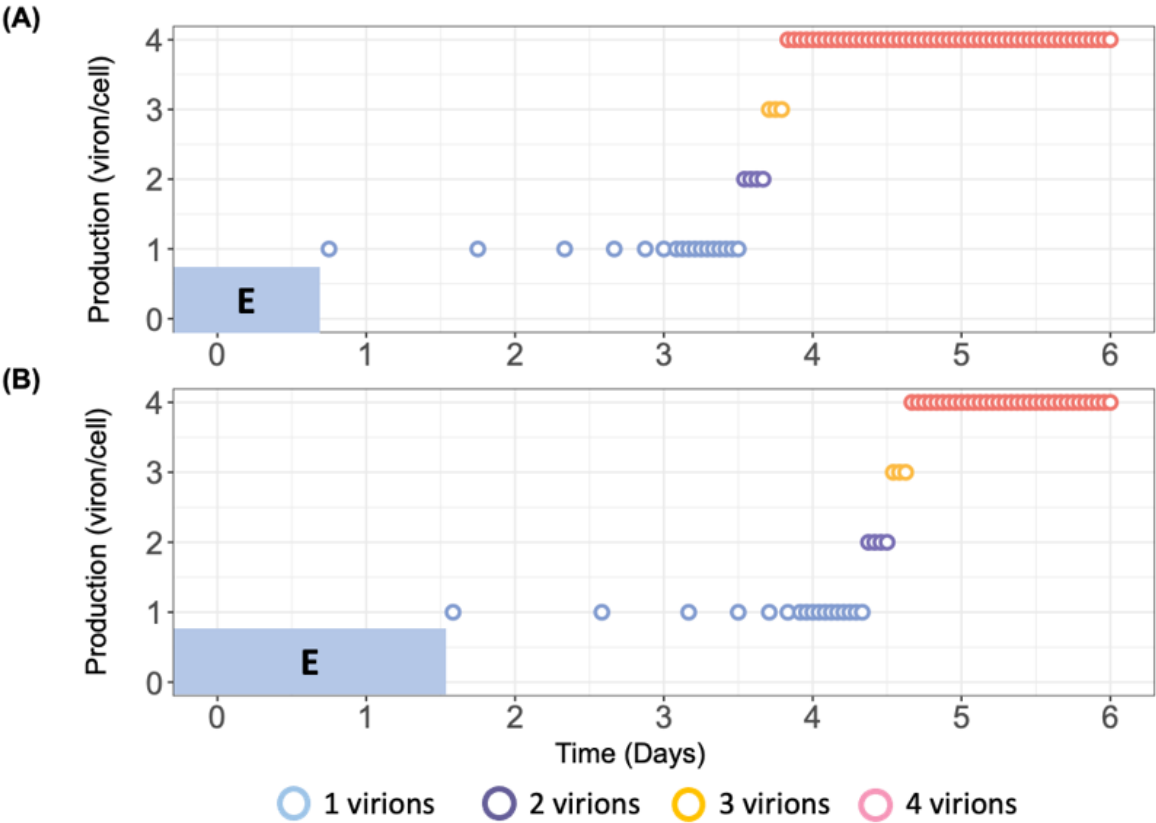
644

Fig. 4. ABM prediction of HBV virion production cycles in PHHs. Blue-shaded "E" represents minimal eclipse phase **(A)** and maximal eclipse phase **(B)** for PHHs. Each PHH has a randomized eclipse phase following by a consistent virion production pattern starts with 1 virion/day. As virus resources accumulate, the production cycle shortens. Production also increases to 2, and then 3 virions before reaching steady state of 4 virions/hr. The magnitude of virion production was calculated using **Eq. 1** and the time between each production cycle was calculated using **Eq. 2**. The parameter values (α, P_{st}, γ, δ, ω) used to calibrate **Eq. 1** and **Eq. 2** were the median level of estimated parameters (**Table 4**).
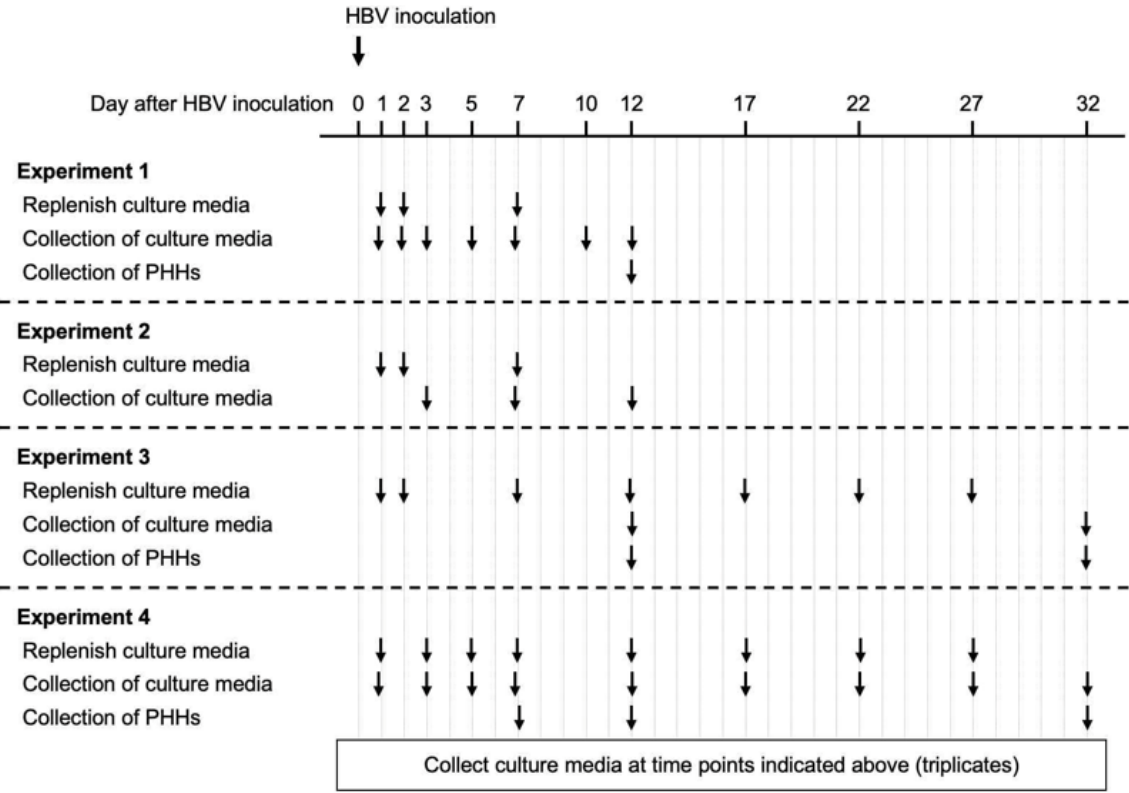
656

Fig. 5. Experimental design for PHHs. PHHs were treated with an inoculum of 10 HBV GEq/cell (Exp 1-3) or 1 HBV GEq/cell (Exp 4) for 1 day, starting on day 0. Myr-preS1 (6.25 µg/mL) treatment was initiated one day after inoculation and then continued throughout the experiment. Extracellular HBV DNA and intracelluar HBV DNA were measured in collected culture media at the indicated time points for each experiment. PHHs were harvested for estimating HBV infected cells. During the infection, culture media was renewed after HBV inoculation or until the end of the experiment as indicated by arrows.
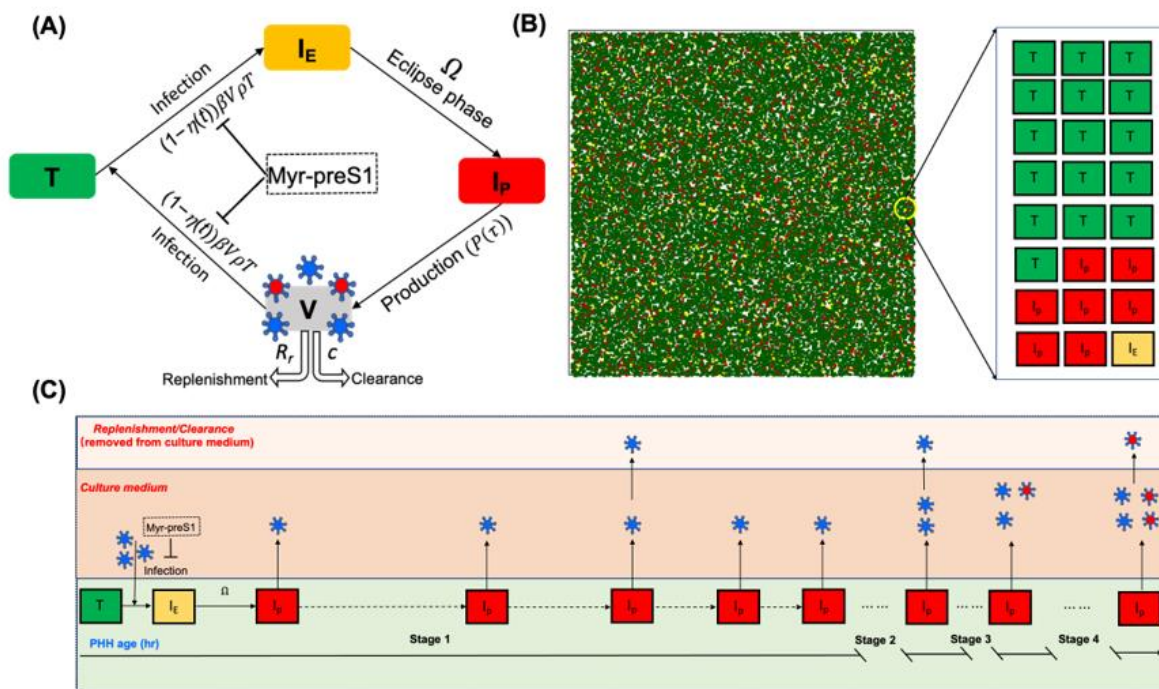
Fig. 6. Conceptualiztion of the agent-based model. (A) The human hepatocytes can be only in one of the following three phases at a given time; T = uninfected cells which are termed as target or susceptible cells, I_E = HBV-Infected cells in eclipse phase (i.e., not yet releasing virions), I_P = HBV-infected cells actively producing/releasing virions. Once I_E become I_p, they produce free virus that can further infect T. The free virus in blood, V, is composed of infectious (red center virus) and non-infections virions (blue center virus). The parameter ρ represents the fraction of virions that are infectious, β represents the infection rate constant, Ω represents eclipse phase duration, $P(\tau)$ represents virion secretion from I_P (**Eq. 1**), c represents viral clearance from blood, R_r represents the portion of virions removed during medium change/replenishment, and we assume no death/loss for PHHs in the culture media. The effectiveness of Myr-preS1 is η when the drug takes effect at t_{eff}. **(B)** Simulated hepatocytes including T (green), I_E (yellow), and I_P (red) in ABM at 15 days after HBV inoculation. **(C)** Schematic diagram of a representative hepatocyte progressing through ABM. Each individual hepatocyte has its own infection kinetics followed by a randomized eclipse phase and viral production cycle (Ω + Stage 1 + Stage 2 + Stage 3 + Stage 4). The virions were initially released by I_P starting with a long production cycle of 1 virion per cell (Stage 1: ~0-2.5 days) that gradually reaches a production of 2 virions per cell with a shorten production cycle (Stage 2: ~2.5-3 days) and then proceeds to 3 virions per cell (Stage 3: ~3-4 days) before virion production increases to reach to a steady state production rate of 4 virions per hour per cell (Stage 4: ~ 4 days onwards).

36

691 **Supplemental Material**

692 **Table S1.** Experimental data (simulated targets) for Exp. 4
693

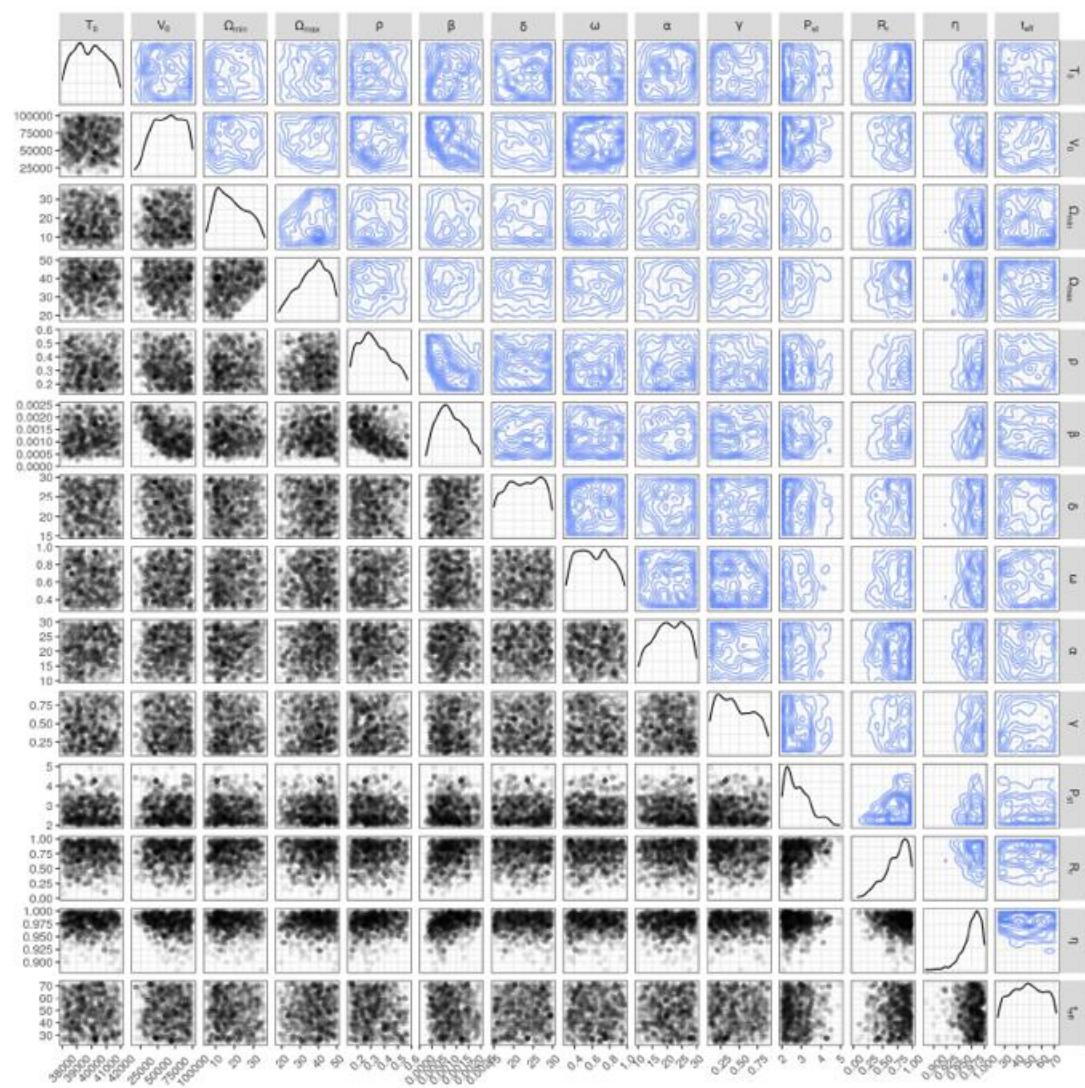| Day	Extra HBV-median [min, median, max]	Percentage of HBV infected cells [min, median, max]
1	[4.595, 5.339, 5.915]	
3	[4.603, 5.106, 5.542]	
5	[3.994, 4.634, 5.184]	
7	[4.384, 5.050, 5.604]	[0, 0.0005, 0.01]
12	[5.443, 6.021, 6.504]	[0.015, 0.02, 0.035]
17	[5.941, 6.644, 7.146]	
22	[6.291, 7.034, 7.627]	
27	[6.758, 7.304, 7.823]	
32	[7.178, 7.696, 8.131]	[0.742, 0.810, 0.854]

694

695
696

Fig. S1. Joint posterior distributions of non-intervention and Myr-preS1 intervention parameters from IMABC (1000 samples). The upper (contour plots) and lower (scatter plots) triangles show the two-dimensional joint posterior distributions. The diagonal shows the marginal distributions of each parameter in **Table 3**.